Analyst

PAPER

View Article Online
View Journal | View Issue

Cite this: *Analyst*, 2019, **144**, 649

A label-free immunosensor for the detection of nuclear matrix protein-22 based on a chrysanthemum-like Co-MOFs/CuAu NWs nanocomposite†

Siyuan Li,‡ Song Yue,‡ Chao Yu, Yiyu Chen, Dong Yuan and Qiubo Yu *

In this study, a new, simple, and label-free electrochemical immunosensor was presented for the detection of nuclear matrix protein-22 (NMP-22). In order to accurately monitor very small amounts of NMP-22, it was advantageous to use highly efficient nanomaterials as signals. For this reason, we synthesized a chrysanthemum-like nanocomposite (Co-MOFs/CuAu NWs), using Co-based metal–organic frameworks (Co-MOFs) as carriers and copper gold nanowires (CuAu NWs) wrapped around their surface, which was applied for modifying a glassy carbon electrode (GCE). The Co-MOFs/CuAu NWs possessed outstanding catalytic capabilities, which served as signal materials and simultaneously carried the anti-NMP-22 antibody (Ab). When different concentrations of the NMP-22 antigen (Ag) were specifically attached to the immunosensor, the current responses decreased by varying degrees. The designed biosensor used the principle to establish a linear regression equation and achieve an accurate quantification of NMP-22. After optimization, the NMP-22 sensor exhibited a good linear response over a concentration range from 0.1 pg mL^{-1} to 1 ng mL^{-1}, with a lower detection limit of 33 fg mL^{-1} (based on S/N = 3). The proposed biosensor demonstrated the advantages of ultra-sensitivity, high specificity and acceptable reproducibility, suggesting that the proposed strategy has the potential for the quantification of NMP-22 in human urine samples. Moreover, the novel nanocomposite Co-MOFs/CuAu NWs are promising materials for electrochemical sensors to detect other biomolecules.

Received 16th August 2018,
Accepted 31st October 2018

DOI: 10.1039/c8an01590b

rsc.li/analyst

Introduction

Bladder cancer (BC) is one of the most frequently diagnosed types of cancer, which possesses high prevalence and recurrence rates.[1–3] For tumor detection and monitoring the recurrence or progression of BC, the current standard methods are urinary cytology and cystoscopy.[4] However, urinary cytology is restricted by its low sensitivity, and cystoscopy is limited by its invasive and costly nature.[5] Nuclear matrix protein-22 (NMP-22), which is a potential biomarker for BC diagnosis and prognosis, controls chromatin regulation and cell separation during replication. The quantification of NMP-22 can be used to monitor tumor recurrence and progression in clinical BC superficial patients and for individualized follow-ups.[6–8] Presently, the quantification of NMP-22 is mainly dependent on enzyme-linked immunosorbent assay (ELISA).[9] Although the sensitivity of the NMP22 ELISA method is relatively good, it is time-consuming, and requires complicated preparation, and thus cannot meet the needs of large-scale and rapid detection. Therefore, it is vital to develop a highly sensitive, non-invasive, simple and economical strategy for the detection of BC. As an alternative method to the conventional procedures, electrochemical immunosensor approaches, employing antibodies as capture molecules and which can quantitatively measure the electrical signals that arise when antibodies bind with the target molecules, have been widely used for clinical diagnosis.[10–12] Moreover, label-free immunosensors are a very attractive type of sensor, which can detect antigen–antibody binding by monitoring the changes in the electronic or interfacial properties.[13] Based on the above reasons, we intend to use label-free immunosensors to achieve a rapid quantitative analysis of NMP-22.

In the past research studies, nanowires had more space to accommodate proteins, which showed exceptional performance for the label-free detection technology in particular.[14,15] Being a new type of high-efficiency electrocatalyst, network-structured nanomaterials have been widely recognized because

Institute of Life Science, Chongqing Medical University, Chongqing 400016, P.R. China. E-mail: yqb76712@gmail.com; Fax: +(86) 23-68865186; Tel: +(86)23 -68815186

†Electronic supplementary information (ESI) available. See DOI: 10.1039/c8an01590b

‡Siyuan Li and Song Yue contributed equally to this work.

of their good catalytic performance and simple synthesis.[16,17] Compared with individual materials, one-dimensional bimetallic nanowires can offer much higher electrical conductivity, and Au-based bimetallic nanomaterials possess superior catalytic activity characteristics.[18–20] In addition, Cu, which is an economical transition element that is abundant in the earth, has the ability to regulate the electrocatalytic properties of catalysts.[21,22] Bimetallic CuAu nanowires produced *via* a simple method (one-step synthesis method) possess excellent catalytic activity, which makes them well suited for sensors. Therefore, this work is about the use of CuAu nanowires to achieve the detection of target substances. In order to increase the sensitivity of this type of sensor, a nanomaterial having a large specific surface area is required as a carrier to support a large amount of CuAu nanowires.

Metal–organic frameworks (MOFs), as a type of host matrix material, have significant advantages, including high specific surface areas, outstanding thermal stability, exposed active sites, and the corresponding structured nanoscale cavities.[23,24] The applications of MOFs have spread to many industrial, environmental, and biological fields, including gas purification and separation, drug delivery, catalysis, and sensing.[25,26] Moreover, cobalt-based MOFs (Co-MOFs) have slowly been gaining popularity and are starting to be applied in sensors.[27] Therefore, the flower-like Co-MOFs synthesized using our proposed strategy, which are advanced materials with a large surface area, have a very comprehensive application prospect. Until now, using MOFs as carriers to anchor other nanoparticles was a relatively frequently used technique, such as when using MOFs to assemble silver nanoparticles, encapsulate hemin, and fix gold nanoparticles.[28–30] To the best of our knowledge, there has barely been any research in which Co-MOFs were prepared as nanowire carriers to be applied in sensors. Owing to the large surface area of Co-MOFs, a large amount of CuAu nanowires can be loaded *via* Au–NH_2 bonds, resulting in stronger catalytic activity. In this work, we synthesized a chrysanthemum-like nanocomposite Co-MOFs/CuAu NWs, with Co-MOFs as the carriers and the CuAu nanowires wrapped around their surface, and applied them in an immunosensor. A label-free immunosensor decorated with a Co-MOFs/CuAu NWs nanocomposite with outstanding catalytic activity was realized, which is critical for detecting a wider range of NMP-22 molecules.

We report on a relatively simple, ultrasensitive, innovative, and label-free electrochemical sensor for NMP-22 detection, using the aforementioned Co-MOFs/CuAu NWs nanocomposite. First, different from that of other composite materials, the synthesis process of the Co-MOFs/CuAu NWs nanocomposite was relatively simple. Secondly, the prepared Co-MOFs/CuAu NWs nanocomposite was not only used as the electrode modification but also acted as signal materials. In the presence of H_2O_2, the Co-MOFs/CuAu NWs nanocomposite produced the same function as that of horseradish peroxidase (HRP), which catalyzed the oxidation of H_2O_2 immediately. Finally, this is the first report of the Co-MOFs/CuAu NWs nanocomposite synthesized and applied in an electrochemical sensor. In order to achieve superior manufacturing, we tested the analytical performance of the proposed biosensor, which has the potential to be further developed and become a powerful technological tool for analyzing other biomolecules.

Experimental section

Materials and chemicals

A human NMP-22 ELISA kit was purchased from Shanghai Yuanye Bio-Technology Co., Ltd (Shanghai, China). 2-Amino terephthalic acid (NH_2–BDC), *N*,*N*-dimethylformamide (DMF), potassium ferrocyanide ($K_4[Fe(CN)_6]$), potassium ferricyanide ($K_3[Fe(CN)_6]$) and copper chloride ($CuCl_2$) were obtained from Sigma-Aldrich (St Louis, USA). Gold chloride solution ($HAuCl_4$) and glucose were purchased from Aladdin (Shanghai, China). Sodium borohydride ($NaBH_4$) was purchased from KeLong Chemical Co. (Chengdu, China). Cobalt nitrate ($Co(NO_3)_2{\cdot}6H_2O$), ascorbic acid, uric acid and hemoglobin were purchased from Sangon Biotech (Shanghai) Co., Ltd (Shanghai, China). Lysozyme was obtained from Solarbio Life Science (Beijing, China). Urea and creatinine were bought from Shanghai Macklin Biochemical Co., Ltd (Shanghai, China). Bovine serum albumin (BSA) was obtained from Aladdin (Shanghai, China). Healthy urine (obtained after informed consent) was provided by the First Affiliated Hospital of Chongqing Medical University (Chongqing, China). The other reagents used in the tests were of analytical grade and no other purification measures were undertaken. All of the water used in our strategy was obtained from a Millipore Mill-Q purification system (>18.2 MΩ cm, USA).

Apparatus and characterization

The electrochemical detection tests were performed using a conventional three-electrode system. The electrochemical experiments of this study, including the cyclic voltammetry (CV) tests and the measurement of amperometric *i*–*t* curves, were carried out using a CHI660E electrochemical workstation (Shanghai Chenhua Apparatus Corporation, China). A glassy carbon electrode (GCE, 4 mm in diameter) was used as the working electrode, whereas a saturated calomel electrode (SCE) was used as the reference electrode and a platinum wire was used as the auxiliary electrode. The morphologies of the Co-MOFs and the Co-MOFs/CuAu NWs nanocomposite were characterized *via* field emission scanning electron microscopy (FE-SEM, JEOL JSM-6700F, Japan). Energy dispersive X-ray spectroscopy (EDS) measurements were carried out employing an Oxford X-max50 microscope (Oxford, England). Using an Al Kα X-ray (1486.6 eV) light source, X-ray photoelectron spectroscopy (XPS) measurements were carried out using a Thermo Scientific ESCALAB 250 Xi spectrometer (Thermoelectricity Instruments, USA).

Synthesis of the Co-MOFs

The Co-MOFs were synthesized according to the literature with slight modifications.[27] First, 218.3 mg of $Co(NO_3)_2{\cdot}6H_2O$ and

81.5 mg of NH_2–BDC were dissolved in 4 mL of DMF, and were then ultrasonicated for 15 min. Afterwards, the mixture was heated in a silicone oil bath at 140 °C for 20 min. The precipitated Co-MOFs were obtained *via* centrifugation (8000 rpm) for 5 min and were washed three times with ultrapure water. Finally, the collected powders were dried at 60 °C for approximately 12 h for further use.

Synthesis of the Co-MOFs/CuAu NWs nanocomposite

Co-MOFs/CuAu NWs nanocomposites were synthesized according to the previous literature with a slight modification.[31] First, 4 mg of $NaBH_4$ was dissolved in 2 mL of ultrapure ice water and poured into 15 mL ultrapure ice water under magnetic stirring (500 rpm). Next, 2 mL of a solution containing 1 mg of Co-MOFs, 1.54 mg of $CuCl_2$, and 90 μL of $HAuCl_4{\cdot}3H_2O$ (5%, w/v) was added to the previous solution within 15 s. The reaction under magnetic stirring continued for 5 min at room temperature. Finally, the resulting nanocomposites were washed with ultrapure water three times and dried under vacuum at 37 °C.

Fabrication of the electrochemical NMP-22 sensor

The fabrication procedure of the label-free immunosensor is shown in Scheme 1. Before the modification, the glassy carbon electrode (GCE) was pretreated carefully using alumina polishing powders with sizes of 0.3 μm and 50 nm for 5 min, respectively. Then, it was sonicated consecutively with water and anhydrous ethanol for 5 min. After the electrode was dried, 10 μL of the Co-MOFs/CuAu NWs nanocomposite solution was added to the surface of the cleaned GCE and dried at room temperature. Subsequently, 8 μL of NMP-22 antibody (Ab) were combined with Co-MOFs/CuAu NWs *via* Au–NH_2 bonds and incubated for 1 h at 37 °C. Next, to eliminate non-specific adsorption, the electrode was coated with a BSA solution (1%, w/v) at room temperature for 30 min. It was worth noting that the electrode was rinsed softly with ultrapure water after each step. Finally, the fabricated electrode was stored in a refrigerator (4 °C) for the following experiments.

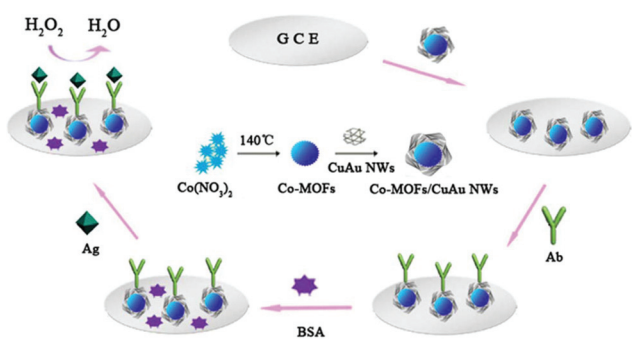

Scheme 1 Fabrication process of the proposed label-free electrochemical immunosensor.

Measurement procedure

8 μL of NMP-22 with a series of different concentrations were added onto the fabricated biosensor, which was then incubated for another 2 h at 37 °C. As before, the electrode was lightly rinsed with ultrapure water to remove unbound compounds. After this step, the sensor was allowed to dry under air at room temperature. The electrochemical *i*–*t* curve was recorded using −0.4 V as the starting voltage, and the three-electrode system was placed in 5 mL of phosphate buffered saline (0.1 M, pH 7.4) at room temperature. Under constant soft stirring, when the background current was stable (after approximately 50 s), 20 μL of H_2O_2 were added to the PBS. The current change was obtained using the following formula: Δcurrent = current − current0, where current represents the current generated when H_2O_2 was added into the PBS, and current0 represents the background current.

Results and discussion

Choice of materials

Compared with single metal catalysts, numerous bimetallic nanomaterials have been developed and used because bimetallic catalysts have been proven to have superior catalytic efficiency in many cases.[32,33] The CuAu nanowires can be used as alternative materials for electrochemical sensors because of their strong catalytic activity and excellent specific surface area. The MOFs, being 3D porous materials, possess a larger specific surface area that immobilizes more biomolecules and can also adsorb abundant redox species, resulting in strong current signals and high sensitivity.[34] Based on the above reasons, we combined the advantages of CuAu nanowires and Co-MOFs to synthesize Co-MOFs/CuAu NWs and used them to detect NMP-22. In Fig. 1, the curves shown represent the respective amperometric responses of bare GCE (curve a), Co-MOFs (curve b), CuAu NWs (curve c), and the Co-MOFs/CuAu

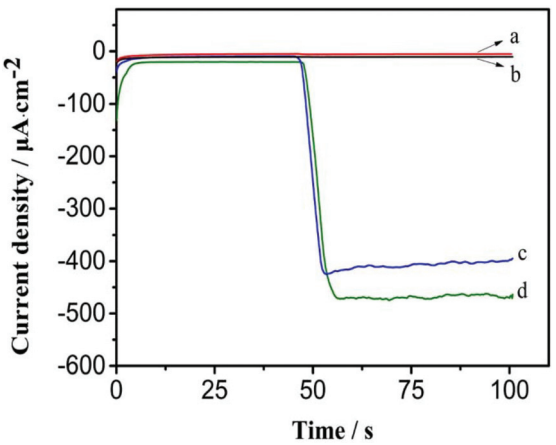

Fig. 1 The *i*–*t* responses of different materials in PBS after adding the same concentration of H_2O_2: (a) bare GCE; (b) Co-MOFs; (c) CuAu NWs; (d) Co-MOFs/CuAu NWs.

NWs nanocomposite (curve d) when 20 μL of H_2O_2 was added in 5 mL of PBS (pH 7.4). The bare GCE (curve a) did not have any electrocatalytic properties. The Co-MOF (curve b) modified electrodes did not possess almost any electrocatalytic properties. As for the CuAu NW modified electrodes, their catalytic signal was markedly higher (curve c). Most notably, a higher signal appeared when Co-MOFs/CuAu NWs (curve d) were used as a coating on the electrodes due to the synergy of Co-MOFs and CuAu NWs. In addition, we incubated the same concentration of antibodies on different materials and the results are shown in ESI Fig. S1.† The results show that the current of the Co-MOFs/CuAu NWs decreased the most when the same concentration of antibodies got attached, indicating that the number of antibodies attached was also the highest. Therefore, the resulting nanocomposite (Co-MOFs/CuAu NWs) was an optimal material for fabricating the desired biosensor.

Morphological and structural characterization of the nanocomposite

FE-SEM was employed to determine the sizes and morphologies of the various materials synthesized in the experiment. As shown in Fig. 2A, most of the Co-MOFs had flower-like structures, which were in accordance with a previous report.[27] After CuAu NWs were synthesized on the surface of Co-MOFs, chrysanthemum-like structures of the Co-MOFs/CuAu NWs nanocomposite (Fig. 2B) were observed, unlike the structures of the Co-MOFs. In addition, elemental analysis of the Co-MOFs and Co-MOFs/CuAu NWs composites was performed using EDS, and the results are shown in Fig. 2C and D. In the EDS image of the Co-MOFs (Fig. 2C), the elemental peaks of the C, O, and Co elements were very clear, indicating the presence of Co in the Co-MOFs. In the EDS image of the Co-MOFs/CuAu NWs complex (Fig. 2D), the elemental peaks of the C, O, Cu, Au, and Co elements were clearly visible and the ratio of each element is shown in ESI Table S1,† indicating that CuAu NWs successfully bound to Co-MOFs. To further confirm the successful synthesis of the nanocomposite, XPS was employed to detect the Co-MOFs/CuAu NWs nanocomposite and the results are shown in ESI Fig. S2.†

Electrochemical behavior of the modified electrodes

After each process, the Co-MOFs/CuAu NWs immunosensor could verify the success of each step by the current *i*–*t* curve. As shown in Fig. 3A, for the bare GCE (curve a), there was no electrocatalytic current response to H_2O_2 at all. The current response of the electrode modified by this material was significantly increased (curve b) because of the strong catalytic ability of the Co-MOFs/CuAu NWs compared with that of the bare electrode. However, the current decreased successively after the antibody (curve c) and BSA (curve d) were stepwise-coated onto the Co-MOFs/CuAu NWs nanocomposite because the transmission of electrons was hindered by the proteins. Finally, due to the specific antigen–antibody reactions, a lower current was obtained when the antigen was attached to the electrode (curve e) which hindered the transmission of the electrons even further.

Meanwhile, the performance of the fabricated label-free immunosensor was measured *via* CV at room temperature. In a 5 mM $[Fe(CN)_6]^{3-/4-}$ solution containing 0.1 mol L^{-1} of KCl, CV measurements were performed at a scan rate of 50 mV s^{-1} ranging from – 0.1–0.6 V. As shown in Fig. 3B, a pair of distinct reversible redox peaks represented the bare GCE (curve a).

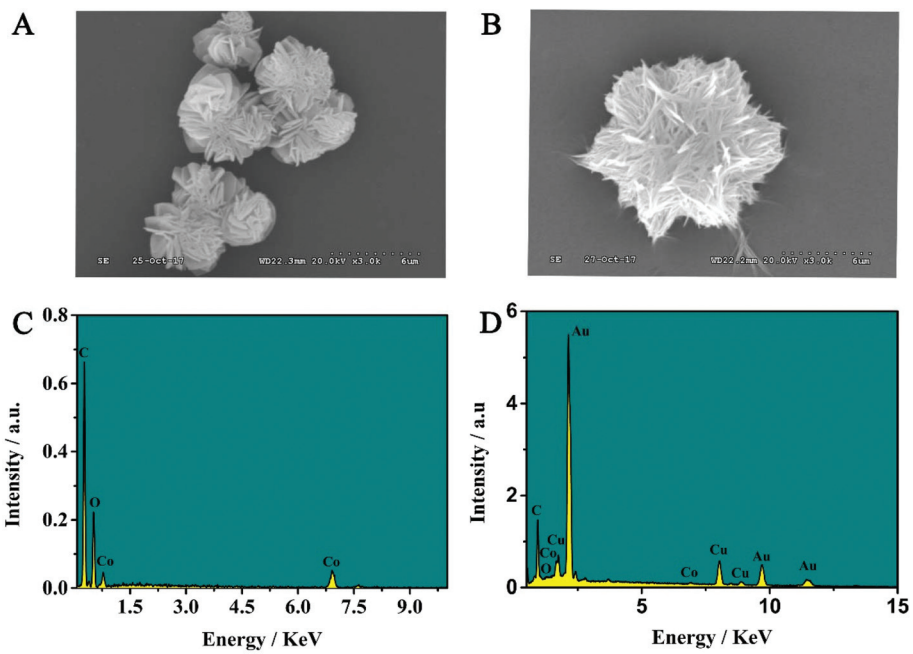

Fig. 2 (A) FE-SEM images of Co-MOFs. (B) Chrysanthemum-like Co-MOFs/CuAu NWs. (C) EDS images of Co-MOFs. (D) EDS images of Co-MOFs/CuAu NWs.

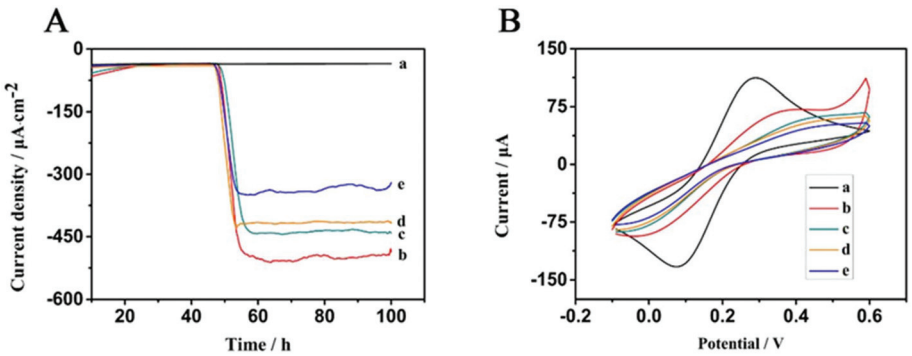

Fig. 3 For each coating stage: (A) *i–t* responses of the electrodes at −0.4 V in the 5 mM PBS solution (pH 7.4) and (B) CV curves of the electrodes in the 5 mM $[Fe(CN)6]^{3-/4-}$ solution: (a) bare GCE; (b) Co-MOFs/CuAu NWs/GCE; (c) anti-NMP-22/Co-MOFs/CuAu NWs/GCE; (d) BSA/anti-NMP-22/Co-MOFs/CuAu NWs/GCE; (e) target/BSA/anti-NMP-22/Co-MOFs/CuAu NWs/GCE.

After the modification of the Co-MOFs/CuAu NWs nanocomposite on the GCE, the peak current declined (curve b) as a result of the relatively weak conductivity of the nanocomposite. Subsequently, the antibodies (curve c) and BSA (curve d) were dropped onto the electrode step by step; the peak current decreased gradually due to the poor conductivity of proteins which could block the electron transfer process. Finally, the peak value (curve e) became lower when the antigen–antibody immunocomplex structures formed, indicating the successful establishment of the label-free immunosensor.

Optimization of the experimental conditions

To prepare highly sensitive and efficient label-free biosensors, it was necessary to optimize the following crucial experimental parameters: (a) the concentration of Co-MOFs/CuAu NWs, (b) the concentration of H_2O_2, (c) the incubation time of anti-NMP-22, and (d) the reaction time between NMP-22 and anti-NMP-22. Fig. S3 (in the ESI†) shows the optimal experimental conditions: (Fig. S3A†) a Co-MOFs/CuAu NWs concentration of 1.5 mol mL^{-1}; (Fig. S3B†) an H_2O_2 concentration of 1.6 mol mL^{-1}; (Fig. S3C†) an incubation time of 45 min for anti-NMP-22; and (Fig. S3D†) a reaction time of 2 h between anti-NMP-22 and NMP-22.

Analytical performance of the NMP-22 sensor

To assess the sensitivity and the quantitative range of the proposed immunosensor, the sensor was incubated with a series of concentrations of NMP-22 under the optimal experimental conditions. The amperometric *i–t* curve was obtained at −0.4 V by adding 20 μL of H_2O_2. As shown in Fig. 4A, when the concentration of NMP-22 was increased from 0.1 pg mL^{-1} to 1 ng mL^{-1}, the current decreased gradually. A good linear dependence between the logarithm of the NMP-22 concentrations and the current responses was observed within the range from 100 fg mL^{-1} to 1 ng mL^{-1}, with an extremely low detection limit reaching 33.3 fg mL^{-1} (S/N = 3). The linear regression equation obtained can be expressed as $Y = 291.333 - 25.938 \times \log C$, with an R squared correlation of 0.994, manifesting a good linear relation (Fig. 4B). By comparing the dynamic linear range and the detection limit of this immunosensor with an existing NMP-22 sensor as shown in Table S2 (in the ESI†), it can be seen that our design strategy resulted in a wider detection range and that the detection limit was relatively lower. These results could be attributed to the Co-MOFs/

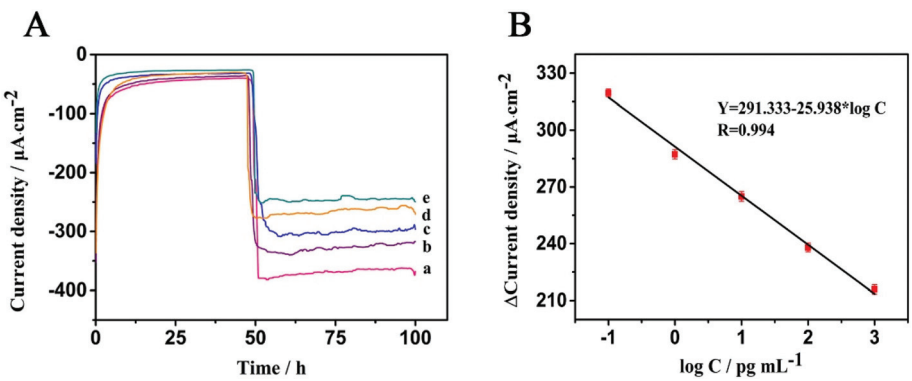

Fig. 4 (A) The *i–t* curve signal results of the immunosensor for the determination of a series of different concentrations of NMP-22: (a) 0.1 pg mL^{-1}; (b) 1 pg mL^{-1}; (c) 10 pg mL^{-1}; (d) 100 pg mL^{-1}; (e) 1 ng mL^{-1}. (B) The calibration curves of the NMP-22 sensor (n = 3).

CuAu NWs, which have an excellent catalytic efficiency and large surface area. In addition, in our experiment, the standard curves were tested using the reagents of the ELISA kit. The results are shown in Fig. S4 (in the ESI†). Compared with the ELISA method, the sensor we designed had a wider linear range, lower detection limits, and higher sensitivity. Therefore, the NMP-22 immunosensor had better performance and more advantages. Additionally, our method is efficient and simple and can be operated relatively easily.

Specificity, stability and repeatability of the NMP-22 sensor

For demonstrating that the designed immunosensor could specifically detect NMP-22, we chose different interfering substances including creatinine, urea, glucose, BSA, ascorbic acid, uric acid, lysozyme, and hemoglobin. Under the same optimal experimental conditions, the specificity of the sensor was investigated using NMP-22 (100 pg mL^{-1}) and interfering substances (1 μg mL^{-1}). As shown in Fig. 5A, the high concentration interferences and the blank control group all maintained a relatively high current, and there were no significant differences between them. Meanwhile, compared with the interfering substance, the NMP-22 group and the mixed group exhibited a significantly lower current response. These results demonstrate that the selectivity of the proposed immunosensor was acceptable.

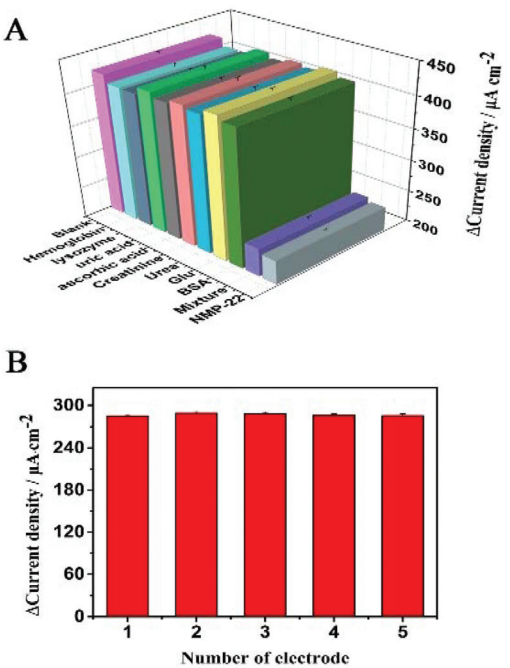

Fig. 5 (A) Different interfering substances were used to test the specificity of the proposed immunosensor: 100 pg mL^{-1} target NMP-22, 1 μg mL^{-1} BSA + 1 μg mL^{-1} Glu + 1 μg mL^{-1} urea + 1 μg mL^{-1} creatinine + 1 μg mL^{-1} ascorbic acid + 1 μg mL^{-1} uric acid + 1 μg mL^{-1} lysozyme + 1 μg mL^{-1} hemoglobin + 100 pg mL^{-1} NMP-22 mixture solution, 1 μg mL^{-1} BSA, 1 μg mL^{-1} Glu, 1 μg mL^{-1} urea, 1 μg mL^{-1} creatinine, 1 μg mL^{-1} ascorbic acid, 1 μg mL^{-1} uric acid, 1 μg mL^{-1} lysozyme, 1 μg mL^{-1} hemoglobin and zero analyte. (B) Repeatability results for five groups of identical electrodes (n = 3) incubated with the same concentration of NMP-22 (1 pg mL^{-1}).

Table 1 The recovery of NMP-22 in human urine samples

Sample	Add	Founded	RSD (%)	Recovery (%)
1	100 fg mL^{-1}	97.12 fg mL^{-1}	0.18	97.12
2	10 pg mL^{-1}	10.08 pg mL^{-1}	0.22	100.85
3	1 ng mL^{-1}	1.02 ng mL^{-1}	0.72	101.67

To assess the stability of the immunosensors, three designed biosensors were conserved in a refrigerator (4 °C) under the same conditions. The current signal was recorded by the amperometric i–t curves after 28 days. Compared with the initial value, the current signal remained at 89.0%. These results revealed that the designed biosensor had outstanding stability within 28 days.

Additionally, the repeatability of the proposed immunosensor was estimated under the same conditions at room temperature. The same concentration of NMP-22 (1 pg mL^{-1}) was detected using five identical groups of NMP-22 immunosensors. As shown in Fig. 5B, the relative standard deviation (RSD) was 0.612%. The experimental data obtained manifested the good repeatability of the proposed immunosensor.

Analysis of the NMP-22 spiked human urine samples

In order to further study the reliability and potential applications of the fabricated immunosensor in an actual sample, the recovery of different concentrations of NMP-22 in human urine samples was carried out *via* the standard addition method. First, the urine was diluted 100-fold using ultrapure water. Then, the NMP-22 was diluted to 0.1, 10, and 1000 pg mL^{-1} by 100 times dilution of human urine. Finally, we measured the currents for different concentrations of NMP-22 and the amperometric i–t curves are shown in ESI Fig. S5.† The collated data are shown in Table 1; the obtained recovery ranged from 97.12% to 101.67% and the variation of the RSD ranged from 0.18% to 0.72%, which implies that the label-free immunosensor exhibited satisfactory accuracy. By testing, this method had considerable capacity for the detection of NMP-22 in real human urine samples.

Conclusions

In summary, a novel electrochemical immunosensor for the quantitative detection of NMP-22 was successfully constructed using Co-MOFs/CuAu NWs as signal amplification materials. The proposed Co-MOFs/CuAu NWs nanocomposite possessed a superior catalytic ability for the reduction of H_2O_2, which was beneficial for sensitivity and to obtain a wide range of detection. Featuring an acceptable specificity, great sensitivity, outstanding stability, and good repeatability, the proposed label-free sensor has the potential to precisely detect NMP-22 and other biomarkers for disease diagnostics. However, unfortunately, no matter how we adjusted the temperature and pH,

the sensor could only be used for one test target and could not be recycled. In future work, we intend to overcome this shortcoming and design a simpler and more feasible scheme for the clinical detection of different kinds of molecules.

Conflicts of interest

There are no conflicts to declare.

Acknowledgements

We would like to thank the National Natural Science Foundation of China (No. 81100443), the Chongqing Yuzhong District of Science and Technology Plan Project (No. 20120214), the Chongqing Municipal Health Bureau Research Project (No. 20132151), and the Chongqing Science and Technology Commission Project (cstc2015shmszx0410) for supporting this project. We would like to express our heartfelt gratitude to all those who have helped us in the course of this project.

References

1 R. Chou and T. Dana, *Ann. Intern. Med.*, 2010, **153**, 461–468.
2 M. Burger, W. Oosterlinck, B. Konety, S. Chang, S. Gudjonsson, R. Pruthi, M. Soloway, E. Solsona, P. Sved, M. Babjuk, M. A. Brausi, C. Cheng, E. Comperat, C. Dinney, W. Otto, J. Shah, J. Thurof, J. A. Witjes and C. International Consultation on Urologic Disease-European Association of Urology Consultation on Bladder, *Eur. Urol.*, 2013, **63**, 36–44.
3 M. Burger, J. W. Catto, G. Dalbagni, H. B. Grossman, H. Herr, P. Karakiewicz, W. Kassouf, L. A. Kiemeney, C. La Vecchia, S. Shariat and Y. Lotan, *Eur. Urol.*, 2013, **63**, 234–241.
4 K. K. Pasikanti, K. Esuvaranathan, P. C. Ho, R. Mahendran, R. Kamaraj, Q. H. Wu, E. Chiong and E. C. Chan, *J. Proteome Res.*, 2010, **9**, 2988–2995.
5 B. Tetu, *Mod. Pathol.*, 2009, **22**(Suppl. 2), S53–S59.
6 S. Jeong, Y. Park, Y. Cho, Y. R. Kim and H. S. Kim, *Clin. Chim. Acta*, 2012, **414**, 93–100.
7 J. K. M. Unoki, D. E. Neal, B. A. J. Ponder, Y. Nakamura and R. Hamamoto, *Br. J. Cancer*, 2009, **101**, 98–105.
8 S. F. Shariat, C. Zippe, G. Ludecke, H. Boman, M. Sanchez-Carbayo, R. Casella, C. Mian, M. G. Friedrich, S. Eissa, H. Akaza, I. Sawczuk, V. Serretta, H. Huland, H. Hedelin, R. Rupesh, N. Miyanaga, A. I. Sagalowsky, F. Wians Jr., C. G. Roehrborn, Y. Lotan, P. Perrotte, S. Benayoun, M. J. Marberger and P. I. Karakiewicz, *J. Urol.*, 2005, **173**, 1518–1525.
9 C. W. Yihhsin Chang, Y. Lee, P. Huang, Y. Kao and M. Shiau, *Adult Urol.*, 2004, **64**, 687–692.
10 D. M. Kim, H. B. Noh, D. S. Park, S. H. Ryu, J. S. Koo and Y. B. Shim, *Biosens. Bioelectron.*, 2009, **25**, 456–462.
11 V. Mani, B. V. Chikkaveeraiah, V. Patel, J. S. Gutkind and J. F. Rusling, *ACS Nano*, 2009, **3**, 585–594.
12 I. H. Cho, J. Lee, J. Kim, M. S. Kang, J. K. Paik, S. Ku, H. M. Cho, J. Irudayaraj and D. H. Kim, *Sensors*, 2018, **18**, 207–225.
13 S. Loyprasert, P. Thavarungkul, P. Asawatreratanakul, B. Wongkittisuksa, C. Limsakul and P. Kanatharana, *Biosens. Bioelectron.*, 2008, **24**, 78–86.
14 A. Mulchandani and N. V. Myung, *Curr. Opin. Biotechnol.*, 2011, **22**, 502–508.
15 Y. Zhang, A. Kolmakov, Y. Lilach and M. Moskovits, *J. Phys. Chem. B*, 2005, **109**, 1923–1929.
16 S. Guo, D. Li, H. Zhu, S. Zhang, N. M. Markovic, V. R. Stamenkovic and S. Sun, *Angew. Chem.*, 2013, **52**, 3465–3468.
17 S. Guo, S. Zhang, X. Sun and S. Sun, *J. Am. Chem. Soc.*, 2011, **133**, 15354–15357.
18 K. J. Chen, K. Chandrasekara Pillai, J. Rick, C. J. Pan, S. H. Wang, C. C. Liu and B. J. Hwang, *Biosens. Bioelectron.*, 2012, **33**, 120–127.
19 C. C. Kung, P. Y. Lin, F. J. Buse, Y. Xue, X. Yu, L. Dai and C. C. Liu, *Biosens. Bioelectron.*, 2014, **52**, 1–7.
20 N. Wang, Y. Han, Y. Xu, C. Gao and X. Cao, *Anal. Chem.*, 2015, **87**, 457–463.
21 J. W. Wei Hong and E. Wang, *Nano Res.*, 2015, **8**, 2308–2316.
22 A. X. Yin, X. Q. Min, W. Zhu, W. C. Liu, Y. W. Zhang and C. H. Yan, *Chemistry*, 2012, **18**, 777–782.
23 Y. Yu, C. Yu, Y. Niu, J. Chen, Y. Zhao, Y. Zhang, R. Gao and J. He, *Biosens. Bioelectron.*, 2018, **101**, 297–303.
24 L. Q. Yu and X. P. Yan, *Chem. Commun.*, 2013, **49**, 2142–2144.
25 J. S. Hussein Rasool Abid, Ha.-M. Ang and S. Wang, *Int. J. Smart Nano Mater.*, 2013, **4**, 72–82.
26 Y. Zhang, C. Liu, F. Wang, Z. Liu, J. Ren and X. Qu, *Chem. Commun.*, 2017, **53**, 1840–1843.
27 X. Yang, J. Lv, Z. Yang, R. Yuan and Y. Chai, *Anal. Chem.*, 2017, **89**, 11636–11640.
28 Z. Jiang, P. Gao, L. Yang, C. Huang and Y. Li, *Anal. Chem.*, 2015, **87**, 12177–12182.
29 J. Chen, C. Yu, Y. Zhao, Y. Niu, L. Zhang, Y. Yu, J. Wu and J. He, *Biosens. Bioelectron.*, 2017, **91**, 892–899.
30 Y. L. Liu, W. L. Fu, C. M. Li, C. Z. Huang and Y. F. Li, *Anal. Chim. Acta*, 2015, **861**, 55–61.
31 W. Hong, J. Wang and E. Wang, *Nanoscale*, 2016, **8**, 4927–4932.
32 S. Zhang, R. Li, X. Liu, L. Yang, Q. Lu, M. Liu, H. Li, Y. Zhang and S. Yao, *Biosens. Bioelectron.*, 2017, **92**, 457–464.
33 S. Nantaphol, T. Watanabe, N. Nomura, W. Siangproh, O. Chailapakul and Y. Einaga, *Biosens. Bioelectron.*, 2017, **98**, 76–82.
34 Z. Tang and Z. Ma, *Biosens. Bioelectron.*, 2017, **98**, 100–112.